Journal of Atmospheric and Solar-Terrestrial Physics 72 (2010) 781–788

Contents lists available at ScienceDirect

Journal of Atmospheric and Solar-Terrestrial Physics

journal homepage: www.elsevier.com/locate/jastp

A LiDAR study of the effective size of cirrus ice crystals over Chung-Li, Taiwan

Subrata Kumar Das [a,*], Jan-Bai Nee [a], Chih-Wei Chiang [a,b]

[a] Department of Physics, National Central University, Chung-Li, Taiwan
[b] Research Center for Environmental Changes, Academia Sinica, Nan-Kang, Taiwan

ARTICLE INFO

Article history:
Received 9 October 2009
Received in revised form
23 March 2010
Accepted 25 March 2010
Available online 30 March 2010

Keywords:
Cirrus
Lidar
Fall-velocity
Effective size

ABSTRACT

In this paper, we estimated the effective size of ice crystals in cirrus clouds using fall velocity derived from LiDAR (light detection and ranging) measurements at Chung-Li (24.58°N, 121.1°E), Taiwan. Nine shapes of the ice crystals, viz. hexagonal plates, hexagonal columns, rimed long columns, crystals with sector-like branches, broad-branched crystals, stellar crystal with broad arms, side planes, bullet rosettes and assemblages of planar poly-crystals of specific dimensions have been analyzed. The results show that the lidar derived most probable mean effective size of ice crystals is 340 ± 180 μm with a dominant size range of 200–300 μm. The lidar derived mean effective size of cirrus crystals are parameterized in terms of cloud mid-height temperature as well as optical depth. The discussed method will be useful to study the most probable effective size distribution of ice crystals in cirrus cloud.

1. Introduction

Cirrus clouds, which are globally widespread in upper troposphere and lower stratosphere (UTLS) region is a topic of research interest for the past several decades due to their ability to modulate the radiative balance of the earth's atmosphere (Sassen, 2002a). They are composed of non-spherical ice crystals, which have a significant role in cooling and heating of the earth–atmosphere system (Liou, 1986). Earlier studies reported that when the sizes of cirrus crystals are relatively large, then greenhouse effect prevails over solar radiation and it can result in warming. However, if the cirrus is composed of small ice crystals then there will be cooling due to the strong albedo (Liou, 1986, 2005). Thus, characterizing the radiative properties of cirrus clouds, which depends on the size, shape and number of the ice crystals, will significantly improve our understanding on the cirrus formation and their influence on the radiation budget and dynamics in UTLS region.

Several studies investigated ice crystals fall velocities and their relationships with shape, size and altitude of cirrus (Jayaweera and Cottis, 1969; Heymsfield, 1972; Heymsfield and Donner, 1990; Mitchell, 1996; Matrosov and Heymsfield, 2000; Heymsfield and Iaquinta, 2000; Heymsfield, 2003). Jayaweera and Cottis (1969) reported the fall velocities of plate and columnar like ice crystals in cirrus and derived their relationship with crystal size. Heymsfield (1972) studied the terminal velocity of different cirrus crystals shapes (viz, bullet, column, plate, dendrite, stellar and needle) and put forward an empirical relationship for the calculation of the terminal velocity of cirrus crystals using aircraft measurements. Mitchell (1996) estimated the terminal velocities for different shapes of ice crystals based on the classifications of Magono and Lee (1966). They showed that in general, the velocity increases linearly with the particle size. It is worth to note that the fall velocity has a significant role on crystal growth mechanism, lifetime and spatial extent of the clouds (Jayaweera and Cottis, 1969; Heymsfield, 1972; Matrosov and Heymsfield, 2000).

In this work, LiDAR (light detection and ranging) measurements are used to calculate fall velocity, and the relationship of velocity and size is used to estimate the size of the cirrus crystals. Lidar is a potential remote sensing tool for probing the clouds to study their macro- and micro-physical properties with high spatial (space-borne) and temporal (ground-based) resolutions. The lidar technique allows the measurement of the height profiles of backscattering coefficient and an increase in the value from their background atmosphere within a defined altitude range indicates the presence of cloud. In a vertically pointing lidar system, if the height of the cloud is estimated by averaging it for a given time interval, then the heights for two given time periods can be used to find the fall velocity of ice crystals. This procedure is more precise for the ice clouds which are at a higher altitude and whose base descends with terminal velocity. The velocity–size empirical relationship of the form $V_f = AD^B$ (where V_f is the fall velocity of ice clouds estimated using lidar, D is the maximum dimension of ice crystal, and A and B are constants) has been used to estimate the effective size of ice crystals (Mitchell, 1996). Later on, the mean size of ice crystals derived from velocity–size

* Corresponding author. Tel.: +886 3 4227151 × 65358; fax: +886 3 4251175.
E-mail address: skdas@phy.ncu.edu.tw (S. Kumar Das).

1364-6826/$ - see front matter © 2010 Elsevier Ltd. All rights reserved.
doi:10.1016/j.jastp.2010.03.024

empirical relationship will be termed as the effective size of the cirrus ice crystals determined with lidar. In the manuscript, the effective size refers to the effective diameter of the ice crystals.

The central objective of this paper is to determine the most probable effective size of ice crystals in cirrus clouds by considering their fall velocity using ground-based lidar. The paper is organized in the following manner: Section 2 presents the detail of the lidar system. Section 3 describes the methodology and data analysis techniques. The results are discussed in Section 4 and finally a brief summary on the dataset is presented in Section 5.

2. System description

In the present study, we have utilized ground-based lidar system installed at National Central University, Chung-Li (24.58°N, 121.10°E), Taiwan. The transmitter of lidar system employs the second harmonics of the Nd:YAG pulsed laser at 532 nm, and maximum energy of ~100 mJ. The pulse width of the laser is 10 ns and has a pulse repetition frequency of 20 Hz. The transmitter is pointed zenith into the atmosphere and the receiver consists of a Newtonian telescope of 45-cm diameter to receive the backscatter signals, with a field of view of 0.5 mrad. The overlap of the transmitter and the receiver is at ~1.6 km and will not make any difference in the current study as the height of cirrus clouds is higher than that of the overlapping function. A narrow band interference filter centered at 532 nm with a full width at half maximum (FWHM) of 3 nm is used to reject the background noise. The detection of the backscatter signals are made through two photo-multiplier tubes (to measure parallel and perpendicular components of polarization) in photon counting mode with pulse discriminators and are recorded continuously by two multi-channel scalars (MCS). The time-dependent signals measured by MCSs are summed for 1000 laser shots which corresponds to 50 s and transferred into a personal computer automatically giving a vertical resolution of 24 m (dwell time of counting system is 160 ns). The experimental specifications of the lidar system used for the present study are mentioned in Table 1. The operation of the lidar system is mainly at night (~20:00 LT; LT=GMT+8:00 h) because during day time there will be saturation of the detectors due to the solar light. Details system description, calibration and algorithm can be found elsewhere (Chen et al., 2002; Das et al., 2009).

3. Methodology and data analysis

3.1. Identification of cirrus clouds using lidar

The backscattering coefficient of clouds is calculated using Fernald's algorithm (Fernald, 1984), by solving the lidar equation expressed as

$$P(z) = P_L \frac{A_T}{z^2} \beta_{atm}(z) e^{-2\int_0^z \sigma_{atm}(z')dz'} \quad (1)$$

where P and P_L are the power received from a distance z and the laser output energy, respectively; A_T is a constant that accounts for the system optical efficiency, the telescope receiver area, and the photo-multiplier tube (PMT) spectral efficiency; β_{atm} and σ_{atm} are the backscatter coefficient and extinction by atmospheric gases ($\beta_{air}(z)$ and $\sigma_{air}(z)$) and clouds ($\beta_c(z)$ and $\sigma_c(z)$) at the laser wavelength, respectively.

The backscattering ratio, $BR(z)$, is expressed as

$$BR(z) = \frac{\beta_c(z) + \beta_{air}(z)}{\beta_{air}(z)} \quad (2)$$

where the symbols have their usual meaning.

The linear depolarization ratio, $\delta(z)$, is the ratio of the total intensity of the parallel ($P_{/\!/}(z)$) and perpendicular ($P_\perp(z)$) channel and written as

$$\delta(z) = \frac{P_\perp(z)}{P_{/\!/}(z)} \quad (3)$$

The depolarization ratio is used to assess the asymmetry of the particles. For water clouds which are composed of spherical liquid droplets, δ is around zero, whereas cirrus clouds which are composed of non-spherical ice crystals, δ is greater than zero. Thus, the depolarization ratio provides the qualitative information to study the composition of ice and water within the clouds (Sassen and Mace, 2002b).

We have considered the following conditions to determine the cirrus clouds boundary:

(i) The base height of cirrus is defined where $BR \geq 1.5$ and this threshold value should also persist for at least 5 range gates ($\sim 24 \times 5 = 120$ m) so that the top height of cirrus can be marked by considering $BR = 1.5$. This is because, if $BR \geq 1.5$, then cirrus clouds are clearly distinguished from the background noise.
(ii) The base height of cirrus should exceed 8 km because the ambient temperature in this altitude is usually less than -20 °C, since below this temperature the clouds particles are of poly-crystalline pattern (Heymsfield and Platt, 1984).
(iii) The value of δ should be > 0.03, since the molecular depolarization ratio is 0.028, reported by Bodhaine et al. (1999).

The mid-height (M) of clouds is defined by using the weighted mean and is expressed as

$$M = \frac{\int_{z_{base}}^{z_{top}} z \times BR(z)dz}{\int_{z_{base}}^{z_{top}} BR(z)dz} \quad (4)$$

where z_{top} and z_{base} corresponds to cloud top and base heights, respectively.

3.2. Calculation of cirrus optical depth using lidar

The optical depth (τ_c) at the laser wavelength is expressed as

$$\tau_c = \int_{z_{base}}^{z_{top}} \sigma_c(z)dz = \int_{z_{base}}^{z_{top}} S_c(z) \times \beta_c(z)dz \quad (5)$$

where σ_c is the extinction coefficient of cloud, $S_c (\approx \sigma_c/\beta_c)$ is extinction-to-backscatter ratio, commonly as lidar ratio and the other symbols have the same meaning mentioned in Section 3.1. For clouds, the lidar ratio is unknown since the values of $\sigma_c(z)$ and $\beta_c(z)$ are unknown. So for the present analysis, the transmission method has been employed to derive an effective lidar ratio for

Table 1
Specifications of Chung-Li Lidar.

Parameter	Specification
Laser source	Nd:YAG
Wavelength	532 nm (linear polarization)
Pulse energy	30–100 mJ
Pulse width	10 ns
Repetition rate	20 Hz
Detector	Photo-multiplier tube
Interference filter	FWHM 3 nm
Receiver	Newtonian telescope (diameter 45 cm)
Field of view	0.5 mrad
Data acquisition	Multi-channel analyzer (Stanford inst. SR430)
Height resolution	24 m
Time resolution	50 s (1000 laser shots integrated)

cirrus cloud. Details about the retrieval methodology of optical depth and lidar ratio can be found in Das et al. (2009 and references therein).

3.3. Estimation of crystals size using lidar

The composition of cirrus clouds are non-spherical ice particles. Moreover, their fall velocity and orientation depends upon the shape, size and density of the crystals (Hallett et al., 2002). In the present study, we have considered an aerodynamic equation given below to parameterize the fall velocity of ice crystals in terms of the effective size (Mitchell, 1996)

$$V_f = a\nu\left(\frac{2\alpha g}{\rho_a \nu^2 \gamma}\right)^b D^{b(\beta+2-\sigma)-1} \quad (6)$$

where all the units are in cgs. V_f is the fall velocity, ν is the kinematic viscosity ($\nu=\eta/\rho_a$, η is the dynamic viscosity; ρ_a is the density of air), g is the acceleration due to gravity, D is the maximum ice crystal dimension, α, β, γ and σ are the constants (Mitchell, 1996) for specific shape and size (refer Table 2).

In the above Eq. (6), a and b are the coefficient and exponent, respectively, in the power-law equation for Reynolds number (Re) with Best (or Davies) number (X) expressed as (Mitchell, 1996)

$$Re = aX^b \quad (7)$$

From the theoretical studies, Mitchell (1996) estimated $a=0.06049$ and $b=0.831$ with $10<X<585$ ($0.4<Re<12$) and reported that the dependence of 'a' and 'b' on the particle habits within the same intervals of X and Re can be neglected and hence same constant value of 'a' and 'b' is adopted in the present study for different shapes of ice crystals. They also mentioned that the above relation is more common for cirrus ice particles. Matrosov and Heymsfield (2000) used Doppler radar to study ice particles fall velocity and their size using Eq. (7). For the present study, we have also considered Eq. (7).

The height profiles of ρ_a and η are estimated from the temperature and pressure observations, obtained from nearby radiosonde flight. We have taken the values of ρ_a and η for different altitude regions according to the lidar observation. By substituting these values in Eq. (6), V_f is estimated for different ice crystal shapes and the mean value is taken for each shapes. The general expression of V_f for different shapes of the ice crystal are tabulated in Table 2.

The selection for the shapes of ice crystal is based on the particles size dimension as suggested by Mitchell (1996). They reported the relationship among mass, size and cross sectional area for most common cirrus crystal shapes. In the present work, nine different shapes of the ice crystals of specific dimensions, viz. hexagonal plates (HP) ($15\ \mu m \le D \le 100\ \mu m$ and $100\ \mu m \le D \le 3000\ \mu m$), hexagonal columns (HC) ($100\ \mu m \le D \le 300\ \mu m$ and $D \ge 300\ \mu m$), rimed long columns (R) ($200\ \mu m \le D \le 2400\ \mu m$), crystals with sector-like branches (P1b) ($10\ \mu m \le D \le 40\ \mu m$ and $40\ \mu m \le D \le 2000\ \mu m$), broad-branched crystals (P1c) ($10\ \mu m \le D \le 100\ \mu m$ and $100\ \mu m \le D \le 1000\ \mu m$), stellar crystal with broad arms (P1d) ($10\ \mu m \le D \le 90\ \mu m$ and $90\ \mu m \le D \le 1500\ \mu m$), side planes (S1) ($300\ \mu m \le D \le 2500\ \mu m$), bullet rosettes ($200\ \mu m \le D \le 1000\ \mu m$) and assemblages of planar poly-crystals ($20\ \mu m \le D \le 450\ \mu m$) have been analyzed. These shapes of the ice crystals are commonly found in cirrus clouds (Heymsfield and Iaquinta, 2000). Table 2 shows the relation between the ice crystal fall velocity and the range of dimension where it is valid for the respective shape.

3.4. Retrieval error and uncertainties in the calculations

An uncertainty in the retrieval of cloud parameters derived from lidar data depends mainly on the instrument noise, consideration of molecular profile, the initial value for upper limit reference height and the lidar ratio. The signal-to-noise ratio (SNR) at 18 km is usually greater than 200 by integrating 4 signal profiles and thus the retrieval of cloud backscattering coefficient ($\beta_c(z)$) is less than 0.5%. The temperature and density information for the molecular backscattering profile ($\beta_{air}(z)$) have been taken from the radiosonde data and thus the error affecting $\beta_c(z)$ from $\beta_{air}(z)$ is within 0.5% based on Pratt (1985). In the present work, the analysis of cloud layer is usually between 10 and 16 km and the error which is produced by an uncertainty of the initial value of extinction is less than 0.3%, based on the standard deviation of data from the past measurements. An uncertainty in the estimation of lidar ratio is less than 30% and therefore optical depth is derived with uncertainty within 15–30% (Chen et al., 2002). By using the standard propagation error formula and the above uncertainties in the lidar measurements, the estimation of the fall-velocity with lidar has a relative uncertainty of less than about 30%. The measurements of depolarization ratio have an uncertainty of less than 0.5% (Chen et al., 2002).

An uncertainty in the estimation of ice crystals size in cirrus cloud depends on the accuracy of input parameters V_f, η, ρ_a, a, b, α, β, γ and σ. η and ρ_a are estimated from radiosonde data and thus an uncertainty in their measurements is within 0.5% (Pratt, 1985). The constants a and b are related with Reynolds number which are chosen within a relative error of within 5% (Mitchell, 1996). The constants α, β, γ and σ are related with ice crystal projected

Table 2
Fall velocity–size relation derived by using Mitchell (1996) technique. The crystals shape information and the values of constant factor terms (α, β, γ and σ) are taken from Mitchell (1996). HP: hexagonal plates, HC: hexagonal columns, R: rimmed long columns, P1b: crystals with sector-like branches, P1c: broad-branched crystals, P1d: stellar crystal with broad arms, S1: side planes, BR: bullet rosettes, APP: assemblages of planar poly-crystals and D: effective diameter of the ice crystals.

Crystal shape	α	β	γ	σ	Fall velocity–size relation (cm s^{-1})	Applicable to ice crystal diameter D (μm)
HP I	0.00739	2.45	0.24	1.85	$V_f=2.54\times10^3\ D^{1.16}$	$15 \le D \le 100$
HP II	0.00739	2.45	0.65	2.00	$V_f=1.11\times10^3\ D^{1.03}$	$100 \le D \le 3000$
HC I	0.00166	1.91	0.0696	1.50	$V_f=2.05\times10^3\ D^{1.01}$	$100 \le D \le 300$
HC II	0.000907	1.74	0.0512	1.414	$V_f=1.61\times10^3\ D^{0.93}$	$D > 300$
R	0.00145	1.8	0.0512	1.414	$V_f=2.37\times10^3\ D^{0.98}$	$200 \le D \le 2400$
P1b I	0.00614	2.42	0.24	1.85	$V_f=2.18\times10^3\ D^{1.14}$	$10 \le D \le 40$
P1b II	0.00142	2.02	0.55	1.97	$V_f=3.24\times10^2\ D^{0.7}$	$40 \le D \le 2000$
P1c I	0.00583	2.42	0.24	1.85	$V_f=2.08\times10^3\ D^{1.14}$	$10 \le D \le 100$
P1c II	0.000516	1.80	0.21	1.76	$V_f=3.11\times10^2\ D^{0.7}$	$100 \le D \le 1000$
P1d I	0.00583	2.42	0.24	1.85	$V_f=2.08\times10^3\ D^{1.14}$	$10 \le D \le 90$
P1d II	0.000270	1.67	0.11	1.63	$V_f=3.10\times10^2\ D^{0.7}$	$90 \le D \le 1500$
S1	0.00419	2.3	0.2285	1.88	$V_f=1.65\times10^3\ D^{1.01}$	$300 \le D \le 2500$
BR	0.00308	2.26	0.0869	1.57	$V_f=2.86\times10^3\ D^{1.24}$	$200 \le D \le 1000$
APP	0.00739	2.45	0.2285	1.88	$V_f=2.65\times10^3\ D^{1.14}$	$20 \le D \le 450$

area and mass and their values are taken from the earlier studies for different shapes (Mitchell, 1996). They used the above constants to calculate the fall velocity using Eq. (6) within an uncertainty of less than 20%. Therefore, by using standard error propagation, the calculated uncertainty in the retrieval of ice crystals effective size with lidar is less than about 36%.

4. Results and discussion

The lidar has been operated for 202 nights during September 2003–December 2006 and the cirrus clouds were observed on 63 nights in this period. The non-observation nights during the study period are either due to bad weather conditions or the system is designed for specific experiment or logistic problems. Out of these (63 nights) there are about 30 cases where we observed single layer cirrus that has some sedimentation tendency. By this constraint, we have ignored the attenuation of lidar signal since the atmospheric attenuation at 532 nm is negligible. We will present and discuss these 30 cases to study the ice crystals effective size and their fall-out velocity in cirrus clouds.

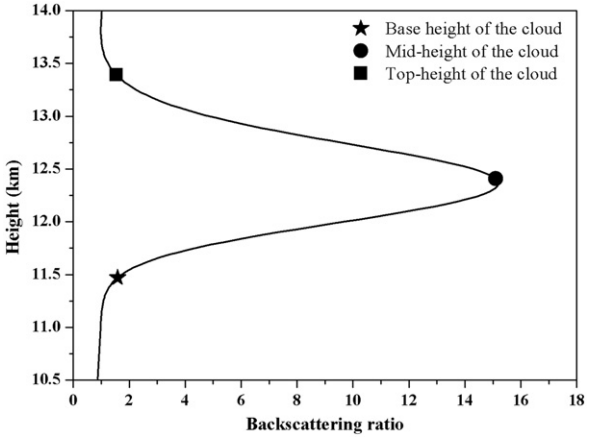

Fig. 1. Height profile of lidar backscattering ratio averaged over 3.3 min (4-scans) on 21 September 2004. Cloud base (star), middle (filled circle) and top (filled square) are also marked.

Fig. 1 displays a typical height profile of BR taken on 21 September 2004, where the cirrus-base, -middle and -top are marked. The profile is averaged for about 3.3 min (4 scans). A three point (72 m) smoothing function is used to remove the small scale fluctuation for all the cases analyzed. The depolarization ratio for the above case is around 0.13, indicating the existences of non-spherical particles. Information about the cirrus occurrence date, mid-cloud temperature along with the depolarization ratio is tabulated in Table 3. Fig. 2 shows the height time intensity (HTI) plot of BR, which indicates the occurrence of cirrus on 21 September 2004. The asterisk in Fig. 2 indicates mid-cirrus cloud height. The least squares method is applied to estimate the sedimentation rate, i.e. the fall-out velocity of ice crystals (Nee et al., 1998; Iwasaki et al., 2004) and the results show that the average fall velocity of the cirrus clouds $\sim$31 cm s^{-1} on 21 September 2004. The middle height of the cirrus clouds is used to calculate the fall velocity. Similar methodology is also adopted for all the 30 cases, to estimate fall-velocity of ice crystals.

It is important to have the background wind information to understand any possible movements of the cirrus cloud over the observational site, though the cirrus clouds can range in horizontal scale of about hundreds of kilometers. Moreover, the horizontal winds could also lead to air mixing, which could increase the evaporation rate of falling particles and thus affect the crystal fall velocity. Fig. 3 (a–d) shows the height profiles of wind speed, wind direction, stability parameter (N^2), and vertical shear of horizontal wind (S^2), respectively, obtained from the radiosonde launched from Banciao (25°N, 121.3°E) at 20:00 LT on 21 September 2004. The horizontal grey area denotes the approximate cirrus cloud layer. Fig. 3 reveals low horizontal wind speed (compared to cirrus fall velocity), very-low vertical wind shear of horizontal wind (S^2) and enhanced static stability parameter (N^2) in the vicinity of the occurrence of cirrus on 21 September 2004. Richardson numbers are also found to be much greater than 1 (not shown) for the foresaid case. Starr and Cox (1980), on the basis of $>$3600 radiosonde ascents, studied upper

Table 3
Properties of cirrus clouds as date of observation, occurrence temperature, depolarization ratio, fall velocity and the size of ice crystals derived with lidar data.

Date (dd-mm-yy)	**Mid-cloud temperature** (K)	**Depolarization ratio**	**Fall velocity** (cm s^{-1})	**Size derived from lidar** (μm)
03-07-2003	211	0.42	26.3	238
06-04-2004	239	0.61	86.2	707
12-05-2004	224	0.21	64.2	561
14-06-2004	215	0.14	24.2	215
06-07-2004	209	0.17	53.3	492
29-07-2004	230	0.16	35.8	343
09-08-2004	214	0.19	27.9	255
30-08-2004	194	0.17	21.8	189
01-09-2004	222	0.19	27.6	251
02-09-2004	228	0.11	26.2	237
06-09-2004	210	0.21	09.5	78
07-09-2004	217	0.20	12.3	102
21-09-2004	223	0.13	31.0	288
02-12-2004	213	0.22	40.2	394
15-03-2005	219	0.26	60.0	601
30-08-2005	201	0.25	25.1	224
02-09-2005	218	0.18	74.5	668
22-09-2005	231	0.22	26.7	242
03-10-2005	209	0.17	13.5	113
31-10-2005	213	0.12	55.7	519
28-06-2006	234	0.12	28.2	258
03-07-2006	222	0.70	28.5	261
04-07-2006	206	0.44	40.5	398
08-08-2006	215	0.15	68.4	604
21-08-2006	216	0.23	28.9	266

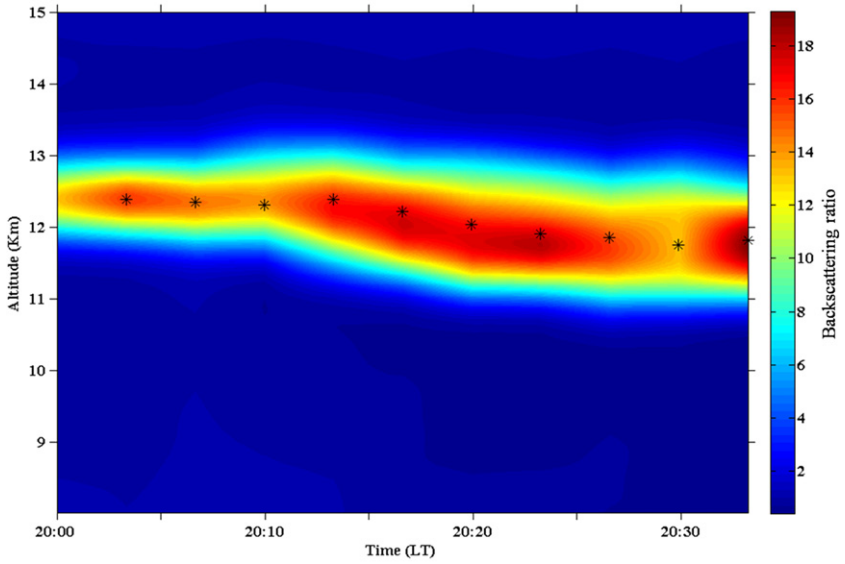

Fig. 2. Height–time intensity plot of lidar backscattering ratio from 20:00 to 20:34 LT on 21 September 2004. Asterisk indicates the mid-cloud height.

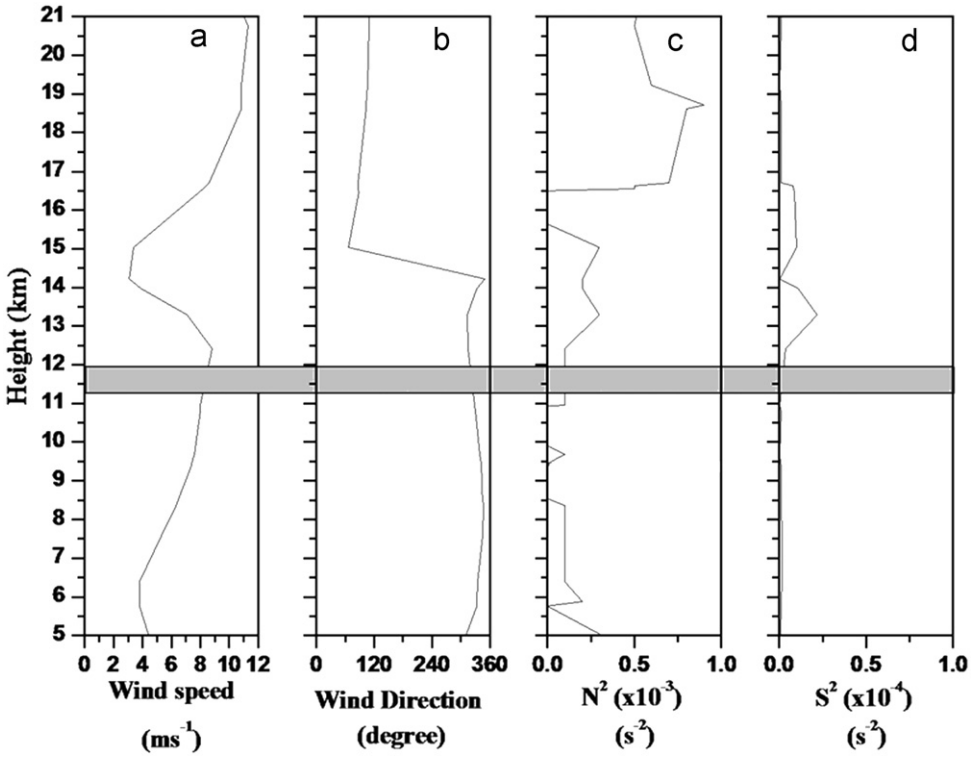

Fig. 3. Height profile of (a) wind speed, (b) wind direction, (c) stability parameter (N^2) and (d) vertical shear of horizontal wind (S^2) derived from radiosonde measurement on 21 September 2004. The grey shaded area represents the approximate cirrus clouds layer.

tropospheric clouds and reported that the thermal stratification of the cloud layer is stable when Richardson numbers are much greater than 1. Thus, the effect of horizontal wind and the shear generated turbulence in the vicinity of cirrus cloud layers for the case described here can be neglected. Since the lidar observation is for a short period (~33 min), the manifestation of atmospheric waves can also be neglected, as the amplitude is far less. The vertical velocity at the vicinity of the cirrus occurrence is confirmed using European Centre for medium-range weather forecasts (ECMWF) model calculation, which also showed much less (cm s^{-1}) values. Thus, the effect of vertical motion is ignored in this case. The above-mentioned conditions are satisfied for 25 cases out of total 30 cases of cirrus observations considered here, where the wind speed and shear are low.

Note that the mid-height of the cloud estimation could be influenced by various local dynamical processes. There could be new nucleation at the cloud top, which could lead to the underestimation of the fall velocity. An increase in relative

humidity at the bottom or decrease in the temperature could results in the overestimation of the fall velocity. However, we restrict our observations to only a time-interval of about 33 min. Within this short span, such physical processes would be negligible to have any significant influence on the velocity estimation. Another uncertainty in the fall velocity estimation could arise in the presence of strong vertical motion through the cloud layer. Such possibilities are minimized by selecting only the lidar measurements during high-pressure system over the study site. Moreover, during the measurement period, the cirrus cloud geometrical thickness is usually within 2 km and thus the survival of ice crystals in cirrus within the measurements time can be ensured (Hall and Pruppacher, 1976).

The effective size of the cirrus ice crystals is estimated by using the general expression for respective shapes tabulated in Table 2. For 21 September 2004, seven shapes of ice crystals (HP II, HC I, P1b II, P1c II, P1d II, BR and APP; for abbreviation and dimension range, refer Table 2) in cirrus have been chosen since the derived size is within the valid dimension range used for the analysis while the remaining shapes have been discarded. The effective size estimated for different shapes and their values are about 309 μm for HP II, 157 μm for HC I, 349 μm for P1b II, 370 μm for P1c II, 372 μm for P1d II, 260 μm for BR and 201 μm for APP. The mean effective size of the ice crystals for this case is about 288 ± 80 μm which is estimated by averaging the size for the seven mentioned shapes.

Similar analysis was carried out for all the selected 25 cases, and the result shows that the mean fall-velocity of the ice crystals in cirrus is around 37 ± 20 cm s^{-1} and their mean effective size is about 340 ± 180 μm. Details of the mean effective size and fall velocity of the ice crystals in cirrus for all the 25 cases are shown in Table 3. Fig. 4 shows the most probable effective size distribution of cirrus ice crystals over Chung-Li. It can be seen that the most probable mean effective size of ice crystals is dominated with the size between 200 and 300 μm. Note that these are habits of only those cases of cirrus when the cirrus ice crystals are mainly distributed among those nine shapes and sizes, mentioned in Section 3.3. Several studies earlier reported that the ice crystals of size between 200 μm and 1 mm usually fall with velocity around 30–100 cm s^{-1} (Mitchell, 1996; Heymsfield, 2003). Gayet et al. (1996), during International Cirrus Experiment (ICE), reported that the particle size distribution of natural cirrus is centered around 375 μm. Recently, Deng and Mace (2008) reported that the majority size of cirrus ice crystals is about several hundred micron and sediments with velocity between 30 and 50 cm s^{-1}. Our results are in agreement with the mentioned literature values.

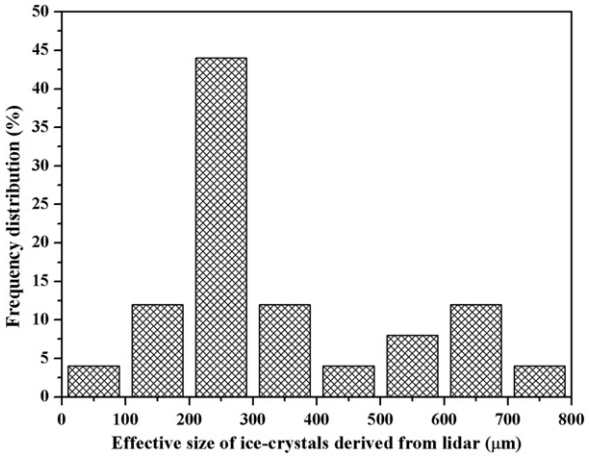

Fig. 4. Most probable effective size distribution of the cirrus ice crystals observed over Chung-Li using lidar measurements.

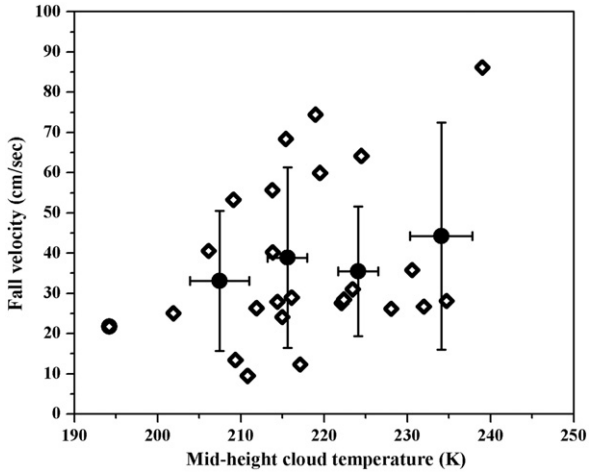

Fig. 5. Scatter plot of fall velocity estimated with lidar versus mid-cloud height temperature. Filled circles represent the averaged velocity with 10 K interval, while the vertical and horizontal bars indicating the standard deviation from their respective mean value.

We carried out further analysis to understand the dependency of the fall velocity and cirrus crystals size on ambient temperature where the cirrus clouds are formed. In order to investigate, the general characteristics of fall velocity estimated from lidar with mid-cloud height temperature, the fall velocity are grouped with an interval of 10 K temperature and averaged. Fig. 5 shows the scatter plot of fall velocity determined with lidar as a function of mid-height cloud temperature. The averaged values of fall velocity at 10 K temperature are also shown with the filled circle. The horizontal and vertical bars represent the standard deviation from their respective mean value. The distribution of the fall-velocity is fairly broad and has a tendency to increase with an increase in the cloud temperature and thus indicating the consequence of particle nucleation. This is in agreement with the observation made by Deng and Mace (2008) from cloud radar over the atmospheric radiation measurement (ARM) site, who reported that the mean fall velocity depends as third order polynomial functions on temperature.

An understanding on the variation of particle size with ambient temperature of cirrus clouds is important since it governs the radiative transfer by the strength of the adiabatic process (Sassen et al., 2003). Fig. 6 shows the temperature dependence of the effective size of ice crystals in cirrus cloud. The temperature is considered at the mid-height of the cloud. Fig. 6 reveals that the effective size of the ice crystals in cirrus usually increases with temperature, consistent with the general behavior of tropical cirrus clouds. This gives an indication that at high altitude with cooler conditions, the size of the ice crystals in cirrus clouds is comparatively smaller. It has been suggested that lower temperature is favorable for homogenous ice-nucleation of small particles because saturation vapor pressure over ice depends exponentially on temperature (Kärcher and Lohmann, 2002; Garrett et al., 2003). Our results are in agreement with Heymsfield and Iaquinta (2000), who reported based on the balloon-borne measurements during First ISCCP Regional Experiment (FIRE), that the size of ice crystals in cirrus increases from lower to higher value with an increase in temperature. Heymsfield and McFarquhar (1996) showed similar results from Central Equatorial Pacific Experiment

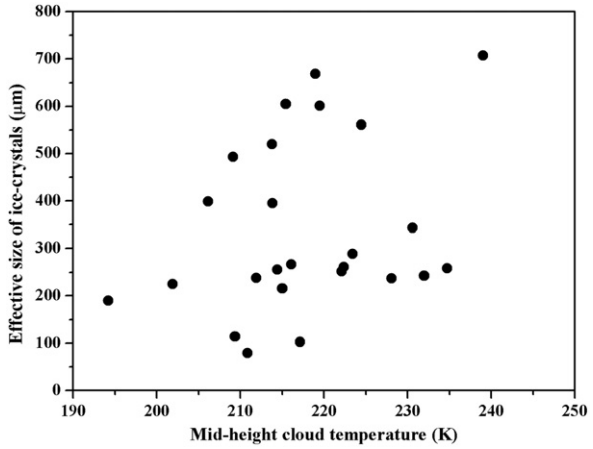

Fig. 6. Scatter plot of effective size of the ice crystals in cirrus with respect to the mid-height cloud temperature.

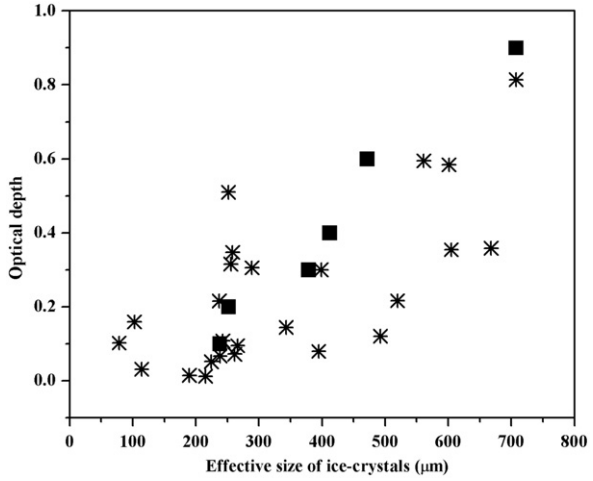

Fig. 7. Scatter plot of optical depth versus effective size of the ice crystals in cirrus. Filled squares represent the averaged values of effective ice crystals size with an interval of 0.1 optical depth.

(CEPEX) and Kwajalein data where they found ice crystals size decreasing with temperature. Also Chen et al. (1997) through observation and model calculation noted a decrease in effective size of ice crystals with ambient temperature over tropical region.

Parameterization of cirrus optical depth with respect to the ice crystals size is needed to examine the sensitivity of climate to cirrus optical properties and its related feedback process. A scatter plot of optical depth with respect to the mean value of effective size of the ice crystals is shown in Fig. 7. Averaged values of effective particle size grouped at an optical depth of 0.1 intervals are also plotted in Fig. 7 as filled squares. In this work, the multiple-corrected optical depth is considered. The effect of the multiple scattering in cloud optical depth is studied with an empirical model provided by Hogan (2006). Fig. 7 shows that the effective size of ice crystals in cirrus has a tendency to increase with an increase of the optical depth. This indicates that an optically thin cirrus clouds are composed of smaller size ice crystals as compared to thick cirrus. The result is in agreement with Wang and Sassen (2002) where they reported that the size of the cirrus ice crystals increases with an increase in the extinction coefficient. The above relationship incorporates an important application in understanding the radiative forcing of cirrus clouds on the atmosphere.

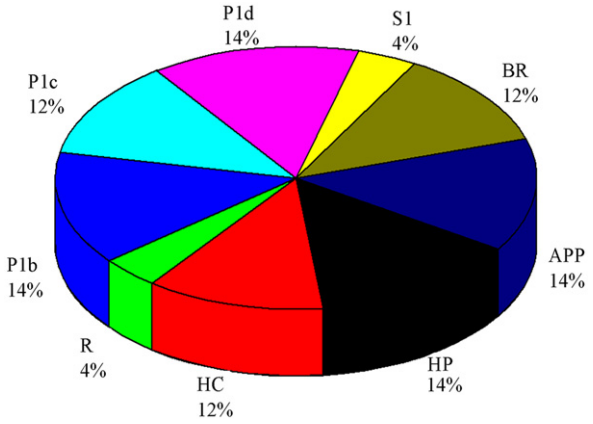

Fig. 8. Percent contribution of different shapes of ice crystals in cirrus observed over Chung-Li, Taiwan. The abbreviation has the same meaning mentioned in Table 2.

It will be quite interesting to study the shape distribution of cirrus ice crystals as it can be useful to understand their scattering properties. One can apply the size distribution to radiative transfer simulations, which can improve the representation of cirrus cloud in weather and climate models. Fig. 8 shows the distribution for the different shapes of the ice crystal in cirrus over Chung-Li. Here in this figure, we have only considered the shape of the ice crystals by clubbing the sizes of same shapes. It is to be noted that the distribution is based merely on probable shapes of the ice crystals considered for this study. It is clearly revealed from the figure that the observed cirrus clouds over Chung-Li has complex composition of HP, HC, P1b, P1c, P1d, BR and APP. Gu and Liou (2006) reported that the inhomogeneity of cirrus cloud composition can perturb the atmospheric warming or cooling rates. Thus the present study indicates the puzzling influence of cirrus on the heating rate of atmosphere over Chung-Li.

5. Summary

Using a 532 nm Nd:YAG lidar, the fall-velocity of cirrus cloud has been calculated and applied to study their shape distribution over Chung-Li, Taiwan during the period of September 2003–December 2006. The least squares method is used to estimate the fall-velocity of ice crystals in cirrus clouds by averaging the cloud height for specific time period ($\sim$33 min). In calculating the fall-velocity, it is considered that the effects of horizontal and vertical wind, shear generated turbulence and atmospheric wave in the vicinity of cirrus layer within the measurement time is negligible and will have minor effect in the present analysis. It is also assumed that the various physical processes such as increase in relative humidity or decrease in temperature would be negligible at the cloud boundaries and will not have any significant influence in their estimation.

A total of 25 cases and nine types of ice crystals shapes are selected for the study. The selection for the most probable shapes of ice crystal is based on the particles size dimension as suggested by Mitchell (1996) and Heymsfield and Iaquinta (2000). Analysis of the result shows that the mean fall-velocity of the ice crystals in cirrus is around $37 \pm 20\ \mathrm{cm\ s^{-1}}$ and their mean effective size is around $340 \pm 180\ \mu\mathrm{m}$. No clear shape dependence has been found and thus indicating a complex ice crystals composition in cirrus over Chung-Li. The fall-velocity of the ice crystals is higher at warmer temperature and thus showing the influence of particle growth or aggregation. The size of the ice crystals in cirrus decrease with decrease in temperature, indicating smaller size at cooler temperature. Optical depth has the tendency to decrease with the decrease in ice crystals size and thus

reveals the manifestation of cloud–radiation interaction. The presented method and results may be used to understand the probable size distribution of ice crystals in cirrus clouds which has an implication on earth's radiation budget.

Acknowledgements

Authors would like to thank Central Weather Bureau (CWB), Taipei, Taiwan for providing radiosonde data for the present study. Thanks are also due to David and Laura of CWB for providing necessary information regarding the soundings. One of the authors (S.K. Das) was supported by a Taiwan scholarship during this study and would like to acknowledge the Taiwan Government and National Central University, Chung-Li, Taiwan.

References

Bodhaine, B.A., Wood, B.N., Dutton, E.G., Slusser, J.R., 1999. On Rayleigh optical depth calculations. Journal of Atmospheric and Oceanic Technology 16, 1854–1861.

Chen, J.-P., McFarquhar, G.M., Heymsfield, A.J., Ramanathan, V., 1997. A modeling and observational study of the detailed microphysical structure of tropical cirrus anvils. Journal of Geophysical Research 102 (D6), 6637–6653.

Chen, W.N., Chiang, C.W., Nee, J.B., 2002. Lidar ratio and depolarization ratio for cirrus clouds. Applied Optics 41, 6470–6476.

Das, S.K., Chiang, C.W., Nee, J.B., 2009. Characteristics of cirrus clouds and its radiative properties based on lidar observation over Chung-Li, Taiwan. Atmospheric Research 93, 723–735.

Deng, M., Mace, G.G., 2008. Cirrus cloud microphysical properties and air motion statistics using cloud radar Doppler moments: water content, particle size, and sedimentation relationships. Geophysical Research Letters 35, L17808, doi:10.1029/2008GL035054.

Fernald, F.G., 1984. Analysis of atmospheric lidar observations: some comments. Applied Optics 23, 652–653.

Garrett, T.J., Gerber, H., Baumgardner, D.G., Twohy, C.H., Weinstock, C.H., 2003. Small, highly reflective ice crystals in low-latitude cirrus. Geophysical Research Letters 30 (21), 2132, doi:10.1029/2003GL018153.

Gayet, J.-F., Febvre, G., Brogniez, G., Chepfer, H., Renger, W., Wendling, P., 1996. Microphysical and optical properties of cirrus and contrails: cloud field study on 13 October 1989. Journal of Atmospheric Science 53, 126–138.

Gu, Y., Liou, K.N., 2006. Cirrus cloud horizontal and vertical inhomogeneity effects in a GCM. Meteorology and Atmospheric Physics 91, 223–235, doi:10.1007/s00703-004-0099-2.

Hallett, J., Arnott, W.P., Bailey, M.P., Hallett, J.T., 2002. Ice crystals in cirrus. In: Lynch, D.K. (Ed.), Cirrus. Oxford University Press, New York, pp. 168–196.

Hall, W.D., Pruppacher, H.R., 1976. The survival of ice particles falling from cirrus clouds in subsaturated air. Journal of Atmospheric Science 33, 1995–2006.

Heymsfield, A.J., 1972. Ice crystal terminal velocities. Journal of Atmospheric Science 29, 1348–1357.

Heymsfield, A.J., Platt, C.M.R., 1984. A parameterization of the particle size spectrum of ice clouds in terms of the ambient temperature and the ice water content. Journal of Atmospheric Science 41, 846–855.

Heymsfield, A.J., Donner, L.J., 1990. A scheme for parameterizing ice cloud water content in general circulation models. Journal of Atmospheric Science 47, 1865–1877.

Heymsfield, A.J., McFarquhar, G.M., 1996. High albedos of cirrus in the tropical Pacific warm pool: microphysical interpretations from CEPEX and from Kwajalein, Marshall Islands. Journal of Atmospheric Science 53, 2424–2450.

Heymsfield, A.J., Iaquinta, J., 2000. Cirrus crystal terminal velocities. Journal of Atmospheric Science 57, 916–938.

Heymsfield, A.J., 2003. Properties of tropical and midlatitude ice cloud particle ensembles. Part I: median mass diameters and terminal velocities. Journal of Atmospheric Science 60, 2573–2591.

Hogan, R., 2006. Fast approximation calculation of multiply scattered lidar returns. Applied Optics 45, 5984–5992.

Iwasaki, S., Tsushima, Y., Shirooka, R., Katsumata, M., Yoneyama, K., Matsui, I., Shimizu, A., Sugimoto, N., Kamei, A., Kuroiwa, H., Kumagai, H., 2004. Subvisible cirrus cloud observation using a 1064 nm lidar, a 95 GHz cloud radar and radiosondes in the warm pool region. Geophysical Research Letters, 31, doi:10.1029/2003GL019377.

Jayaweera, K.O.L.F., Cottis, R.E., 1969. Fall velocities of plate-like and columnar ice crystal. Quarterly Journal of Royal Meteorological Society 95, 703–709.

Kärcher, B., Lohmann, U., 2002. A parameterization of cirrus cloud formation: homogeneous freezing of supercooled aerosols. Journal of Geophysical Research 107 (D2), 4010, doi:10.1029/2001JD000470.

Liou, K.N., 1986. Influence of cirrus clouds on weather and climate processes: a global perspective. Monthly Weather Review 114, 1167–1199.

Liou, K.N., 2005. Cirrus Clouds and Climate. The McGraw Hill Companies.

Magono, C., Lee, C.V., 1966. Meteorological classification of natural snow crystals. Journal of the Faculty of Science, Hokkaido University 2, 321–362.

Matrosov, S.Y., Heymsfield, A.J., 2000. Use of Doppler radar to assess ice cloud particle fall velocity–size relations for remote sensing and climate studies. Journal of Geophysical Research 105, 22427–22436.

Mitchell, D.L., 1996. Use of mass- and area-dimensional power laws for determining precipitation particle terminal velocities. Journal of Atmospheric Science 53, 1710–1723.

Nee, J.B., Len, C.N., Chen, W.N., Lin, C.I., 1998. Lidar observation of the cirrus cloud in the tropopause at Chung-Li (25°N, 121°E). Journal of Atmospheric Science 55, 2249–2257.

Pratt, R.W., 1985. Review of radiosonde humidity and temperature errors. Journal of Atmospheric and Oceanic Technology 2, 404–407.

Sassen, K., 2002a. Cirrus clouds: a modern perspective. In: Lynch, D.K. (Ed.), Cirrus. Oxford University Press, New York, pp. 11–40.

Sassen, K., Mace, G.G., 2002b. Ground-based remote sensing of cirrus cloud. In: Lynch, D.K. (Ed.), Cirrus. Oxford University Press, New York, pp. 168–196.

Sassen, K., Wang, Z., Platt, C.M.R., Comstock, J.M., 2003. Parameterization of infrared absorption in midlatitude cirrus clouds. Journal of Atmospheric Science 60, 428–433.

Starr, D.O'C., Cox, S.K., 1980. Characteristics of middle and upper tropospheric clouds as deduced from rawinsonde data, Atmospheric Science Paper No. 327. Colorado State University, Fort Collins.

Wang, Z., Sassen, K., 2002. Cirrus cloud microphysical property retrieval using lidar and radar measurements. Part II: midlatitude cirrus microphysical and radiative properties. Journal of Atmospheric Science 59, 2291–2302.